Proceedings of PRADS2016
4^{th}-8^{th} September, 2016
Copenhagen, Denmark

Reducing uncertainty of Monte Carlo estimated fatigue damage in offshore wind turbines using FORM

Jan-Tore H. Horn[1)] and Jørgen Juncher Jensen[1,2)]

[1)]Centre for Autonomous Marine Operations and Systems (NTNU AMOS), Norwegian University of Science and Technology (NTNU), Norway
[2)]Department of Mechanical Engineering, Technical University of Denmark (DTU), Denmark

Abstract

Uncertainties related to fatigue damage estimation of non-linear systems are highly dependent on the tail behaviour and extreme values of the stress range distribution. By using a combination of the First Order Reliability Method (FORM) and Monte Carlo simulations (MCS), the accuracy of the fatigue estimations may be improved for the same computational efforts.

The method is applied to a bottom-fixed, monopile-supported large offshore wind turbine, which is a non-linear and dynamically sensitive system. Different curve fitting techniques to the fatigue damage distribution have been used depending on the sea-state dependent response characteristics, and the effect of a bi-linear S-N curve is discussed. Finally, analyses are performed on several environmental conditions to investigate the long-term applicability of this multistep method. Wave loads are calculated using state-of-the-art theory, while wind loads are applied with a simplified model based on rotor thrust coefficients.

Keywords

Fatigue; FORM; monopile; Monte Carlo; reliability; wind turbine.

Introduction

Dynamic structures subjected to stochastic, non-linear environmental loads may require many long simulations to confidently estimate fatigue damage in the design phase (Zwick and Muskulus, 2015). Depending on the degree of non-linearity in the system, computed fatigue may vary significantly between each simulation (Jensen, 2015), and extreme values may have large impact on the expected lifetime estimation. An example is illustrated in Fig. 1 for the mudline fatigue damage on a 10MW monopile mounted offshore wind turbine. The conventional seed averaging method (D_C) is normalized with the true expected damage (D_e).

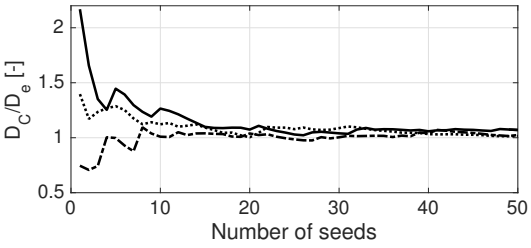

Figure 1. Three example fatigue estimations for 100s simulations with U=6m/s, H_S=1.5m, and T_P=4.7s

It is clear that the results are converging, but are highly dependent on extreme values when the number of seeds are small to moderate. The behaviour is explained by investigating the fatigue damage distribution in Fig. 2. Extreme values are five times greater than the expected value, and the shape indicates a Weibull distribution. The present distribution yields a larger probability of extreme outliers compared to a Gaussian process, leading to slower convergence of the mean value. However, extreme values are also physical and need to be accounted for nonetheless.

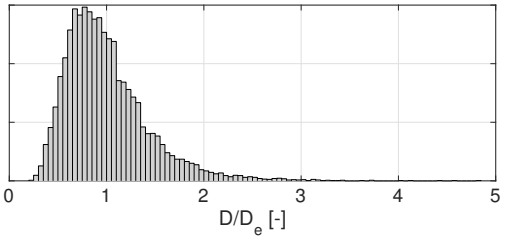

Figure 2. Example fatigue distribution for 10,000 samples with U=6m/s, H_S=1.5m, and T_P=4.7s

The proposed method in Jensen (2015) is to replace the large values with a FORM evaluation of the extremes in the fatigue distribution tail. As a result, outliers are accounted for in each fatigue estimation, but with less impact on the variance. The paper starts with an introduc-

tion to FORM analysis. Then, fatigue damage calculation methods are presented, both conventional, the method from Jensen (2015), and new proposals for representation of the fatigue probability density function (PDF). A detailed descriptions of the procedure and the simulation models are provided, before the verification results are presented.

Background

FORM

The objective of the FORM analysis is to minimize the function

$$G(\mathbf{u}) = D_{ext} - D(\mathbf{u}) \tag{1}$$

to determine the design-point $D(\mathbf{u}^*) \approx D_{ext}$ by a linear approximation. Here, D_{ext} is some extreme fatigue damage and $\mathbf{u} = [\bar{u}_1, \ldots, \bar{u}_m, \tilde{u}_1, \ldots, \tilde{u}_n]$ are standard normal random variables. The conventional Hasofer-Lind (HL) and modified HL (MHL) method as described in Liu and Der Kiureghian (1991), has been used as iteration schemes. The equations to be satisfied at the design-point are (Madsen et al., 1986):

$$G(\mathbf{u}^*) = 0 \tag{2}$$

$$\mathbf{u}^* + \lambda^* \nabla G(\mathbf{u}^*) = 0 \tag{3}$$

where

$$\lambda^* = -\frac{\nabla G(\mathbf{u}^*)\mathbf{u}^*}{|\nabla G(\mathbf{u}^*)|^2} \tag{4}$$

and the gradient is defined as:

$$\nabla G(\mathbf{u}) = \left[\frac{\partial G}{\partial u_1}, \frac{\partial G}{\partial u_2}, \ldots, \frac{\partial G}{\partial u_{m+n}}\right]^T \tag{5}$$

Iterations on $\mathbf{u}$ is based on the function value of (1) and the gradient. The $(k+1)$ iteration point is found from a weighted linear function:

$$\mathbf{u}_{k+1} = \mathbf{a}_k + (1-\xi)\mathbf{d}_k \tag{6}$$

where

$$\mathbf{a}_k = [\mathbf{u}_k \nabla G(\mathbf{u}_k) - G(\mathbf{u}_k)] \frac{\nabla G(\mathbf{u}_k)^T}{|\nabla G(\mathbf{u}_k)|^2} \tag{7}$$

and

$$\mathbf{d}_k = \mathbf{u}_k - \mathbf{a}_k \tag{8}$$

which is illustrated in Fig. 3. For the HL method, $\xi = 1$, so that (6) reduces to $\mathbf{u}_{k+1} = \mathbf{a}_k$. With the MHL method, $\mathbf{u}_k$ is chosen along the line $\mathbf{d}_k$ by stepwise increasing ξ in (6) from 0.2 to 1.0 in order to minimize the following cost function (Liu and Der Kiureghian, 1991):

$$M(\mathbf{u}) = |\mathbf{u} - \frac{\nabla G(\mathbf{u})\mathbf{u}}{|\nabla G(\mathbf{u})|^2}\nabla G(\mathbf{u})|^2 + cG(\mathbf{u})^2 \tag{9}$$

In this particular case, $c \propto (D_{\text{ext}})^{-2}$ has given a reasonable cost function, putting most weight on the last term.

S-N Curves

Fatigue damage is calculated using S-N curves obtained from DNV GL (2005) for a structure in seawater with cathodic protection, and the material parameters obtained are given in Table 1 for a bi-linear curve illustrated in Fig. 4. The fatigue damage is then obtained with a rainflow counting (RFC) method using the WAFO toolbox (WAFO-group, 2000) in MATLAB. The Palmgren-Miner rule for accumulated damage is given as

$$D = \sum_j n_j K_j^{-1} (\text{SCF} \cdot \Delta\sigma_j)^{m_j} \left(\frac{t}{t_{\text{ref}}}\right)^{k \cdot m_j} \tag{10}$$

where $\Delta\sigma_j$ is the rainflow filtered stress range for S-N curve j (Moan and Naess, 2013) and n_j is the rainflow counted number of cycles. The stress concentration factor (SCF) is taken as 1.0, using the base material cross section at the mudline which in this case has a diameter of 8m and thickness of 110mm.

Table 1. Parameters for bi-linear S-N curve

m_1		3.0
m_2		5.0
$\log_{10} K_1$		11.764
$\log_{10} K_2$		15.606
Fatigue limit	[MPa]	52.63
SCF		1.0
t_{ref}	[mm]	25
k		0.2

Fatigue Damage Estimation Using the Reliability Index

The traditional way of calculating the expected fatigue damage is to average over N statistically independent simulations:

$$D_e = \frac{1}{N}\sum_{i=1}^{N} D_i \tag{11}$$

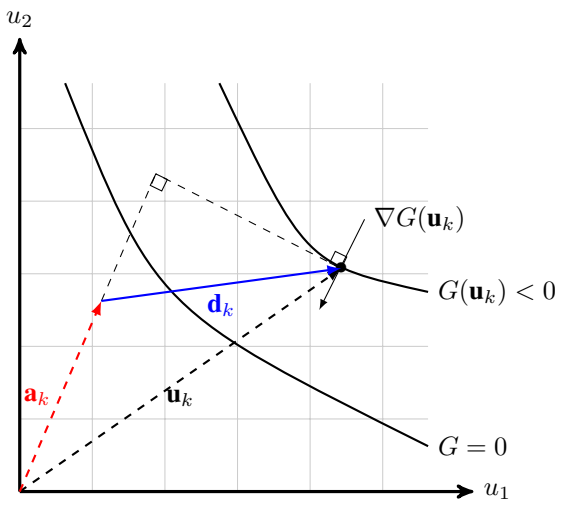

Figure 3. Illustration of FORM iteration

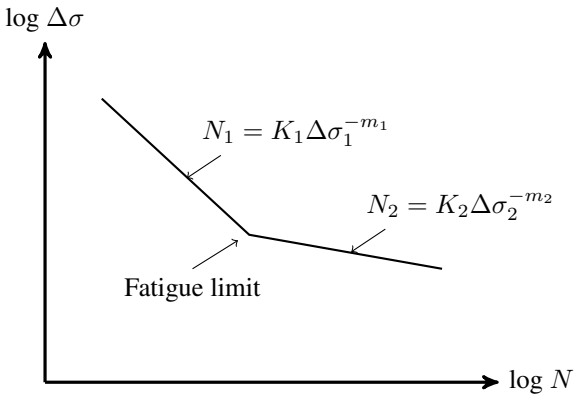

Figure 4. S-N curves above and below the fatigue limit.

which is equivalent to integrating over the PDF of the fatigue damage to get the expected value:

$$D_e = \int_0^\infty Df(D)dD \tag{12}$$

We now define the reliability index β through the standard normal cumulative density function (CDF), Φ:

$$P[D > D_i] = 1 - \frac{i}{N} = \Phi(-\beta_i) \tag{13}$$

resulting in

$$\beta_i = -\Phi^{-1}(P[D > D_i]) \approx -\Phi^{-1}(1 - \frac{i}{N}) \tag{14}$$

for sorted fatigue damage values so that $D_i \leq D_{i+1}$ and $i = 1, 2, .., N-1$. The fatigue damage PDF can now be expressed in terms of β using the formulation in (13):

$$\begin{aligned} f(D) = \frac{dF(D)}{dD} &= 1 - P[D > D_i] \\ &= -\frac{d\Phi(-\beta)}{d\beta}\frac{d\beta}{dD} \\ &= \frac{1}{\sqrt{2\pi}}\exp(-\frac{1}{2}\beta^2)\frac{d\beta}{dD} \end{aligned} \tag{15}$$

Note that we obtain a Gaussian distribution PDF for constant $d\beta/dD$. The expected fatigue damage in (12), can now be re-written as a summation:

$$\begin{aligned} D_e &= \int_0^\infty Df(D)dD \\ &= \frac{1}{\sqrt{2\pi}}\sum_{i=1}^{N} D_i(\beta_i)\exp(-\frac{1}{2}\beta_i^2)\Delta\beta_i \end{aligned} \tag{16}$$

It is clear that $D_e \to \infty$ since $\Delta\beta_N \to \infty$ when using (13). Instead, a linearization of the tail as described in the next section is performed. The first $N-1$ increments in β for the summation are evaluated as:

$$\Delta\beta_i = \begin{cases} \frac{1}{2}(\beta_{i+1} - \beta_i) & \text{for } i = 1 \\ \frac{1}{2}(\beta_{i+1} - \beta_{i-1}) & \text{for } 2 \leq i \leq N-2 \\ \beta_i - \beta_{i-1} & \text{for } i = N-1 \end{cases} \tag{17}$$

Tail Linearization

It is assumed that for large β, the relationship with the fatigue damage is close to linear:

$$D(\beta) = A + B\beta \tag{18}$$

which means that the extreme fatigue damage values follow a Gaussian distribution. As a result, the last term of the summation in (16) for $i = N$, can be written as (Jensen, 2015):

$$\begin{aligned} &\frac{1}{\sqrt{2\pi}}D_N(\beta_N)\exp(-\frac{1}{2}\beta_N^2)\Delta\beta_N \\ &= \frac{1}{\sqrt{2\pi}}\int_{\beta_{N-1}}^\infty D(\beta)\exp(-\frac{1}{2}\beta^2)d\beta \\ &= A(1 - \Phi(\beta_{N-1})) + \frac{B}{\sqrt{2\pi}}\exp(-\frac{1}{2}\beta_{N-1}^2) \end{aligned} \tag{19}$$

which inserted in (16) gives

$$\begin{aligned} D_{SL} = &\frac{1}{\sqrt{2\pi}}\sum_{i=1}^{N-1} D_i(\beta_i)\exp(-\frac{1}{2}\beta_i^2)\Delta\beta_i \\ &+ A(1 - \Phi(\beta_{N-1})) + \frac{B}{\sqrt{2\pi}}\exp(-\frac{1}{2}\beta_{N-1}^2) \end{aligned} \tag{20}$$

where SL denotes a combination of summation and linearization. The constants A and B in (18) is found using the FORM analysis to obtain a sufficiently large extreme fatigue damage D_{ext} and a corresponding reliability index β_{FORM}. An example is shown in Fig. 5 where a linear function is fitted to the tail of the fatigue damage values. This particular case contains 10,000 simulations of simulation time $T_{\text{sim}} = 100$s. A FORM analysis yields the plotted coordinate for a yearly extreme damage and corresponds well to the simulated extremes and the hypothesis of a linear tail i.e. Gaussian distributed. The simulated fatigue damage is converted to an equivalent yearly damage with:

$$D_{\text{year}} = 365 \cdot 24 \cdot 60^2 \cdot \frac{D_{\text{sim}}}{T_{\text{sim}}} \tag{21}$$

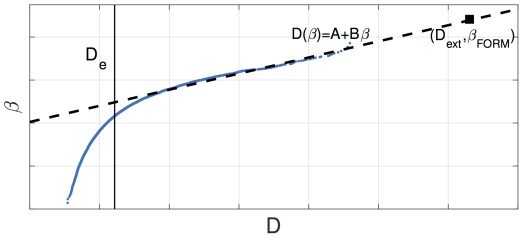

Figure 5. Example linear tail fit

In order to obtain a proper linear fit, a sufficient amount of simulations has to be done. From Fig. 5, it is clear that the coordinate in addition to the FORM-evaluated point has to lie on the linear area of the results, meaning approximately $\beta > 1.2$. Also, since β_N is supposedly large,

the second point has to be (D_{N-1}, β_{N-1}). Finally, combining $\beta_{N-1} > 1.2$ with (14) yields $N > 8$. The coefficients in (18) can now be written as:

$$B = \frac{D_{ext} - D_{N-1}}{\beta_{FORM} - \beta_{N-1}} \tag{22}$$

$$A = D_{N-1} - B\beta_{N-1} \tag{23}$$

Special Case for Gaussian Fatigue Damage

In the special case that the fatigue damage is Gaussian distributed, (18) is a good approximation for $\beta \in \{-\infty, \ldots, \infty\}$. As a result, the expected fatigue damage can be found as:

$$\begin{aligned} D_L =& \int_0^\infty D f(D) dD \\ =& \frac{1}{\sqrt{2\pi}} \int_0^\infty D \exp(-\frac{1}{2}\beta^2) \frac{d\beta}{dD} dD \\ =& \frac{1}{\sqrt{2\pi}} \int_{\beta'}^\infty D \exp(-\frac{1}{2}\beta^2) d\beta \\ =& \frac{1}{\sqrt{2\pi}} \int_{\beta'}^\infty (A + B\beta) \exp(-\frac{1}{2}\beta^2) d\beta \\ =& A \int_{\beta'}^\infty \frac{1}{\sqrt{2\pi}} \exp(-\frac{1}{2}\beta^2) d\beta \\ =& A(1 - \Phi(\beta')) + \frac{B}{\sqrt{2\pi}} \exp(-\frac{1}{2}\beta'^2) \end{aligned} \tag{24}$$

and for $\beta' \to -\infty$:

$$D_L = A \tag{25}$$

Note that B disappears due to the integration of an odd function over the entire domain. The above result means that a good estimate of D_e can be found from only two pairs of (D_i, β_i), and the coefficients in (18) are now:

$$B = \frac{D_2 - D_1}{\beta_2 - \beta_1} \tag{26}$$

$$A = D_1 - B\beta_1 \tag{27}$$

which means that for $\beta' \to -\infty$:

$$D_L = \frac{D_1\beta_2 - D_2\beta_1}{\beta_2 - \beta_1} \tag{28}$$

where $D_2 > D_1$. For a good linear approximation, it is preferred that $D_2/D_1 \gg 1$, therefore, the FORM procedure may be used to find $\beta_2 = \beta_{\text{FORM}}$ for some extreme value of $D_2 = D_{\text{ext}}$. The remaining point for linear regression has to be found by several simulations which is demonstrated in the results section.

Weakly Non-Gaussian Fatigue Damage

Due to the utilization of bi-linear S-N curves, the fatigue damage might be slightly non-Gaussian or Weibull distributed with respect to β, which means that a quadratic polynomial description might be more appropriate than the linear representation in (18):

$$D(\beta) = A + B\beta + C\beta^2 \tag{29}$$

which inserted into (12) yields:

$$\begin{aligned} D_Q =& \int_0^\infty D f(D) dD \\ =& \frac{1}{\sqrt{2\pi}} \int_0^\infty D \exp(-\frac{1}{2}\beta^2) \frac{d\beta}{dD} dD \\ =& \frac{1}{\sqrt{2\pi}} \int_{\beta'}^\infty (A + B\beta) \exp(-\frac{1}{2}\beta^2) d\beta \\ &+ \frac{1}{\sqrt{2\pi}} \int_{\beta'}^\infty C\beta^2 \exp(-\frac{1}{2}\beta^2) d\beta \\ =& A\,(1 - \Phi(\beta')) + \frac{B}{\sqrt{2\pi}} \exp(-\frac{1}{2}\beta'^2) \\ &+ \frac{1}{\sqrt{2\pi}} \int_{\beta'}^\infty C\beta^2 \exp(-\frac{1}{2}\beta^2) d\beta \\ =& A\,(1 - \Phi(\beta')) + \frac{B}{\sqrt{2\pi}} \exp(-\frac{1}{2}\beta'^2) \\ &+ C\left(1 - \Phi(\beta') + \frac{\beta'}{\sqrt{2\pi}} \exp(-\frac{1}{2}\beta'^2)\right) \\ =& (A + C)(1 - \Phi(\beta')) \\ &+ \frac{B + C\beta'}{\sqrt{2\pi}} \exp(-\frac{1}{2}\beta'^2) \end{aligned} \tag{30}$$

and for $\beta' \to -\infty$:

$$D_Q = A + C \tag{31}$$

Typically, one could choose $\beta' = \beta_1$ from simulations. The constants A, B and C are found using a polynomial curve fitting to the data in MATLAB, including the FORM evaluated point which is crucial to obtain stable results for few seeds.

Procedure

The complete procedure for the SL method is summed up as:

1. Perform N simulations with a detailed simulation model and evaluate the first $N - 1$ terms in (16)

2. Use a simplified and computationally efficient model to find β_{FORM} and $\mathbf{u}^*$ for a given $D_{\text{ext}} > D_{N-1}$. It is preferred that $\beta_{\text{FORM}} > 2.5$

3. Do an iteration on the detailed model with $\mathbf{u} = \mathbf{u}^*$ to find an updated D_{ext}, which is valid for the detailed model, but with the same reliability index, β_{FORM}
4. Use the results in 1) and 3) to evaluate (20)

Details regarding the simulation models are given in the next section. The simulation procedure for the simplified model is illustrated in Fig. 6, where the yellow blocks represent codes developed in MATLAB for this particular set-up. First, the FORM-evaluated set of standard normal random variables, $\mathbf{u}$, is transformed to uniform random variables, $\boldsymbol{\epsilon}$, through

$$\boldsymbol{\epsilon} = 2\pi\Phi(\mathbf{u}) \tag{32}$$

in *fatigue.m*. Then, the calculated environmental forces and/or wave elevation from *force.m* are passed on to USFOS where the dynamic simulations are performed. Finally, desired response time-series are returned to MATLAB and *fatigue.m* for post-processing. The damage is then calculated and returned to *FORM.m* for evaluation.

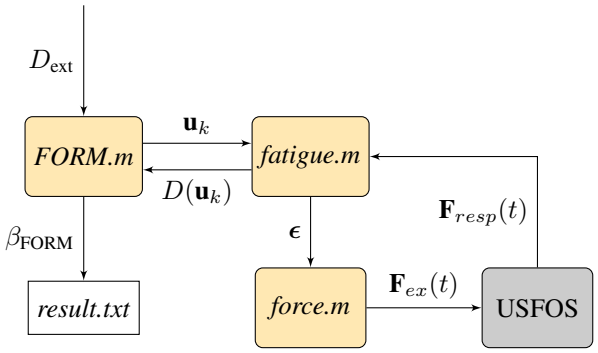

Figure 6. Block diagram of simulation process for the simplified model

Summary of Methods for Fatigue Estimation

The presented methods for fatigue damage calculation are summed up in Table 2.

Table 2. Fatigue calculation methods

Symbol	Formulation
D_C	$\frac{1}{N}\sum_{i=1}^{N} D_i$
D_{SL}	$\frac{1}{\sqrt{2\pi}}\sum_{i=1}^{N-1} D_i \exp(-\frac{1}{2}\beta_i^2)\Delta\beta_i$ $+ A(1-\Phi(\beta_{N-1})) + \frac{B}{\sqrt{2\pi}}\exp(-\frac{1}{2}\beta_{N-1}^2)$
D_L	$A(1-\Phi(\beta_1)) + \frac{B}{\sqrt{2\pi}}\exp(-\frac{1}{2}\beta_1^2)$
D_Q	$(A+C)(1-\Phi(\beta_1)) + \frac{B+C\beta_1}{\sqrt{2\pi}}\exp(-\frac{1}{2}\beta_1^2)$

In this work, it is found that the expressions for D_L and D_Q can be replaced by their asymptotic values in (25) and (31), respectively. This has lead to more stable estimations of the fatigue damage.

Limitation of Variables in FORM Analysis

To speed up the FORM analysis, iterations are only performed on the random variables contributing the most to the fatigue damage. In other words, a sensitivity evaluation based on the first iteration is carried out. The most significant variables are stored in $\mathbf{u}'$ after the first iteration, satisfying:

$$\min\left(\nabla G(\mathbf{u}')\right) > \nu|\nabla G(\mathbf{u}_1)| \tag{33}$$

for some constant ν so that $\mathbf{u}'$ only contains the significant values. Further, $\mathbf{u}_2 = \mathbf{u}'$ implying that the following simulations are only using the variables from $\mathbf{u}'$. For instance, wave components with small frequencies and/or small amplitudes will not have impact on the fatigue damage calculation, and the number of components will depend on the sea-state. In Fig. 7, an example is shown where 7 out of 19 wave components are found to be insignificant. For the disregarded variables, values from the first iteration are used for evaluation of β, and as constants in the remaining simulations. If deterministic wave amplitudes are used, it is assumed that the significant components are grouped.

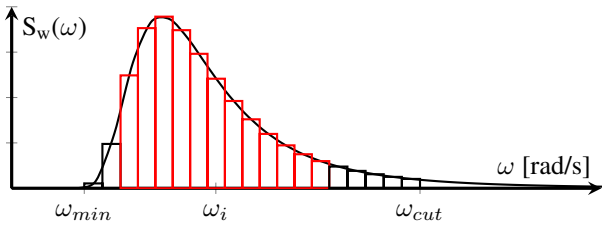

Figure 7. Example discretized wave spectrum with significant wave components in red

Simulation Models

Structural Model

The structural model is a monopile based on the 10 MW DTU reference wind turbine (Bak et al., 2013). The transition piece and pile have a diameter of 8m and thickness of 110mm, and it is located at 30m water depth. The first and second natural periods are 4.8s and 1.0s, respectively. Rotor- and nacelle masses are lumped to the tower top,and the soil layers are modelled as non-linear springs all. An illustration of the model is shown in Fig. 8 with corresponding parameters in Table 3.

To be able to perform the FORM analysis in reasonable time, a simplified model is used for the iterations. This is based on the assumption that the design-point is the same for the detailed and simple model. In other words, a sea-state giving extreme fatigue on the simple model will also give extreme damage on the detailed model. Differences between the models are stated in Table 4. Note

Table 3. Model parameters

H	[m]	115
d	[m]	30
d_s	[m]	42
M	[ton]	675

that the difference in simulation time are not very large, which means that very limited time can be used on the FORM analysis in order to justify the use of the presented method. If a complete wind turbine model including rotor had been used, simulation time would at least be doubled, and the proposed method is even more attractive. However, more work has to be done to find a simple aerodynamic model that matches the complete rotor dynamics by only using a single wind series, like e.g. Smilden and Eliassen (2016).

Table 4. Simulation models

	Detailed	Simple
Elements	21	12
Number of soil springs	26	6
Rotor	No	No
Aerodynamics	C_T	C_T
Hydrodynamics	2nd order	1st order
Controller	None	None
Real time/sim. time [s/s]	0.4	0.2

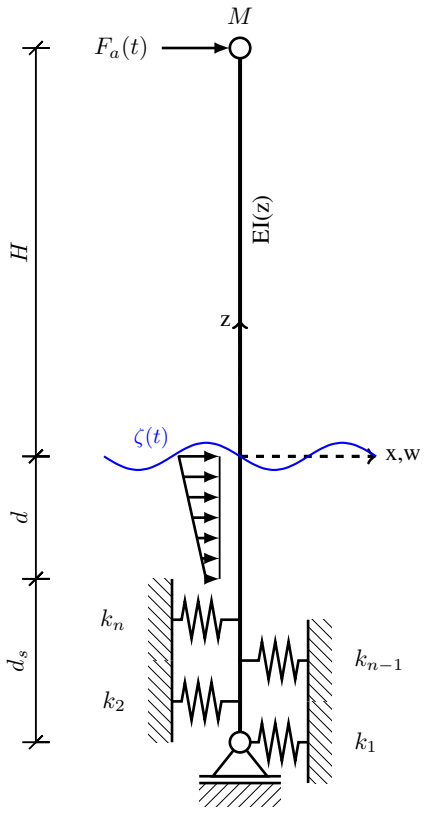

Figure 8. Simplified wind turbine model

Hydrodynamic Loads

The wave elevation in an irregular sea is described with Faltinsen et al. (1995):

$$\zeta(t) = \sum_{i=1}^{m} \sqrt{2S_{\mathrm{w}}(\omega_i)\Delta\omega}\cos(\omega_i t + \bar{\epsilon}_i) \qquad (34)$$

where $\Delta\omega = \frac{2\pi}{T}$ (Zheng et al., 2006) and $\omega_i = \omega_{min} + (i-1)\Delta\omega$. The maximum number of wave components can be found as $m = \frac{\omega_{cut}-\omega_{min}}{\Delta\omega} \leq 0.35T$ when $\omega_{min} = 0.3$[rad/s] and

$$\omega_{cut} = \min\left[2.5, \sqrt{\frac{2g}{H_S}}\right] \qquad (35)$$

Here, the wave amplitudes are deterministic to limit the number of random variables, but they can also be modeled as Rayleigh distributed (Tucker et al., 1984). For small m, this should be done in order to obtain a Gaussian surface elevation. The phase angles are uniformly distributed and obtained from normally distributed variables with (32). For the simple model, only the wave components are given as input to USFOS, which automatically calculates the first order hydrodynamic forces. The detailed model utilizes second order hydrodynamic forces which is pre-calculated in MATLAB and given as a spatially time-variant interpolation grid as input to USFOS. Kinematics calculations are based on an FFT algorithm similar to what is used in Horn et al. (2016). From previous studies (Horn et al., 2016), it has been found that second order wave loads are only significant when $\mathrm{H}_S > 5$, which means that these loads can be neglected in smaller sea-states, which increases the computational efficiency.

Simplified Aerodynamic Thrust Model

The turbulent wind is found by realizing the Kaimal spectrum (DNV GL, 2014):

$$S_{uu}(f) = \sigma_u^2\left(\frac{4L}{\bar{U}}\right)\left(1+\frac{6fL}{\bar{U}}\right)^{-5/3} \qquad (36)$$

where the standard deviation

$$\sigma_u = I(0.75\bar{U}+5.6) \qquad (37)$$

is given as a function of the mean wind speed, $\bar{U}$, and turbulence intensity, I, which is set to 0.14. The total wind speed is then:

$$U(t) = \bar{U} + V(t) \qquad (38)$$

where the gust component, V, is found with:

$$V(t) = \sum_{i=1}^{n} \sqrt{S_{uu}(f_i)\Delta f/\pi}\cos(2\pi f_i t + \tilde{\epsilon}_i) \qquad (39)$$

where $\Delta f = \frac{1}{T}$ and $n = \frac{f_{cut}-f_{min}}{\Delta f} = \frac{1-0}{\Delta f} = T$. Which means that the number of components in the wind gust is equal to the simulation time for a high frequency cut-off of 1Hz. Higher frequencies are excluded to simulate the

low-pass filtering effects of the rotor. The thrust force can now be found using:

$$F_a = \frac{1}{2}\rho_a \pi R^2 C_T(\beta, \lambda) U^2 \tag{40}$$

where C_T is the aerodynamic thrust coefficient dependent on pitch angle (β) and tip-speed ratio (λ), R is the rotor radius and ρ_a is the density of air. Here, it is assumed that the pitch angle, and tip-speed ratio $\lambda = \frac{\omega_R R}{U}$, can be written as functions of the rotor-induced lowpass-filtered wind speed, $\widetilde{U}$, and true wind speed U:

$$\beta \approx \beta(\widetilde{U}) = \begin{cases} 0, & \text{for } \widetilde{U} < U_R \\ \frac{\widetilde{U}-U_R}{1.8\widetilde{U}-6.7}\ [\text{rad}], & \text{for } \widetilde{U} \geq U_R \end{cases} \tag{41}$$

$$\lambda \approx \lambda(U, \widetilde{U}) = \begin{cases} \lambda_{\text{opt}} \frac{\widetilde{U}}{U}, & \text{for } \widetilde{U} < U_R \\ \lambda_{\text{opt}} \frac{U_R}{U}, & \text{for } \widetilde{U} \geq U_R \end{cases} \tag{42}$$

where $\lambda_{\text{opt}} = \frac{\omega_{\max} R}{U_R} = 7.5$ is the optimal tip-speed ratio. The lowpass filtered wind speed is found with:

$$\dot{\widetilde{U}} = \frac{1}{\tau}\left(U - \widetilde{U}\right) \tag{43}$$

for some time constant τ, which has to be tuned according to a more detailed simulation model. It has been found that $\tau = 3$ gives sufficiently accurate thrust for all wind speeds in this case. Now, we introduce a modified thrust coefficient C_T', so that $C_T'(U, \widetilde{U}) = C_T(\beta, \lambda)$. The modified coefficient is plotted in Fig. 9. To accomplish this, the thrust coefficient, $C_T(\beta, \lambda)$ is approximated by the polynomial:

$$\begin{aligned} C_T(\beta, \lambda) \approx\ & a_{00} + a_{01}\lambda + a_{02}\lambda^2 + a_{10}\beta \\ & + a_{20}\beta^2 + a_{11}\lambda\beta + a_{12}\lambda^2\beta + a_{21}\lambda\beta^2 \end{aligned} \tag{44}$$

with the constants for the present turbine given in Table 5. The resulting modified expression for the aerodynamic thrust is then:

$$F_a = \frac{1}{2}\rho_a \pi R^2 C_T'(U, \widetilde{U}) U^2 \tag{45}$$

Table 5. Thrust coefficient parameters

a_{00}	-0.27127
a_{01}	0.19974
a_{02}	-0.007461
a_{10}	0.02822
a_{20}	-5.875e-05
a_{11}	-0.0088
a_{12}	-9.822e-05
a_{21}	-6.342e-05

It should be noted that the presented aerodynamic model is lacking the ability to capture transient load effects and other thrust variations due to the presence of a rotor, but it is considered to be sufficient for this initial study.

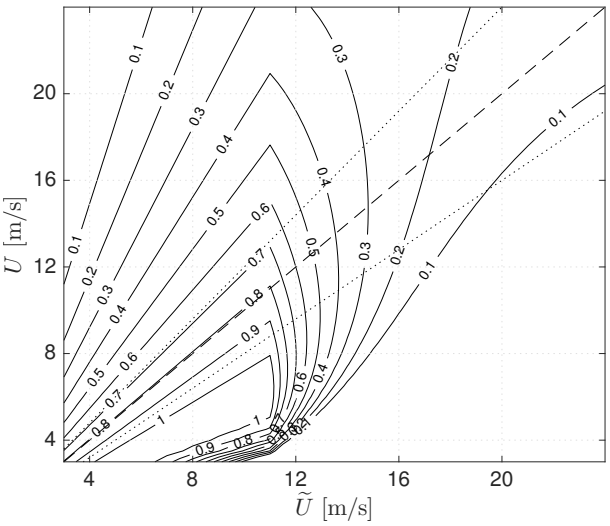

Figure 9. Thrust coefficient, $C_T'(U, \widetilde{U})$, with dashed line for $\widetilde{U} = U$ and dotted lines for the most probable region: $\widetilde{U} = U(1 \pm 0.2)$

Deterministic 3P Effects

To account for thrust variations that oscillates with three times the rotor frequency, given a three-bladed rotor, a deterministic time-series is added to the wind to create an equivalent wind speed. In reality, only the wind shear and tower shadow are deterministic effects, while the rotational sampling of the rotor is stochastic and hence neglected in this case. A sinusoidal function with amplitude of 8% of the instantaneous true wind speed and a frequency of three times the rotor frequency, ω_R, is added:

$$U_{\text{eq}} = U + 0.08U \sin(3\omega_R t) \tag{46}$$

where

$$\omega_R \approx \omega_R(\bar{U}) = \begin{cases} \lambda_{\text{opt}} \frac{\bar{U}}{R}, & \text{for } \widetilde{U} < U_R \\ \lambda_{\text{opt}} \frac{U_R}{R}, & \text{for } \widetilde{U} \geq U_R \end{cases} \tag{47}$$

In other words, the rotational frequency of the rotor is assumed to be close to constant during the simulations, which might result in a slightly unrealistic load excitation at exactly $3\omega_R$.

Aerodynamic Damping

Aerodynamic damping has a great influence on the fatigue damage on the tower and pile. Usually, the aerodynamic damping is accounted for in the structural damping matrix when a simple thrust model is used. Here, the thrust is found through an equivalent drag force on a cylinder at the rotor-nacelle assembly location. The thrust can then be transferred to the tower by a simple drag formulation including relative velocity:

$$F_{a,\text{rel}}(U, \widetilde{U}) = \frac{1}{2}\rho_a D C_D(U, \widetilde{U}) \left[U - V_{\text{RNA}}\right]^2 L \tag{48}$$

Table 6. Sea-states for FLS conditions

No.	H_S [m]	T_P [s]	U [m/s]	p [-]
1	1.5	4.7	6	0.1002
2	3.0	6.2	10	0.0314
3	4.8	7.5	14	0.0092

By Fig. 10 it is clear that this approach is able to represent the expected aerodynamic damping which is reported to be 4-7% in most cases (Burton et al., 2002). When only wave loads are considered, the structural damping is increased from 1 to 5% to account for damping contribution from an operational turbine.

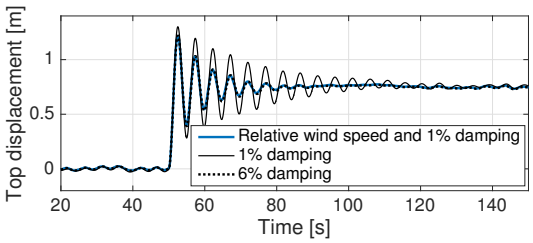

Figure 10. Decay test at 16[m/s] wind speed with structural damping and relative wind speed comparison

Random Variables

The total uniform random variables from wind and waves are collected as

$$\boldsymbol{\epsilon} = [\bar{\boldsymbol{\epsilon}}, \tilde{\boldsymbol{\epsilon}}] \tag{49}$$

where $\bar{\boldsymbol{\epsilon}} = [\bar{\epsilon}_1, ..., \bar{\epsilon}_m]$ are wave component phase angles and $\tilde{\boldsymbol{\epsilon}} = [\tilde{\epsilon}_1, ..., \tilde{\epsilon}_n]$ are wind component phase angles, if used.

Results

The three sea-states considered are shown in Table 6 and represents typical FLS conditions at Dogger Bank along with their probability of occurrence, p.

When only wave loads are used, the aerodynamic damping is accounted for by increasing the structural damping to 5%. The damping is applied as Rayleigh damping with proper coefficients to obtain the wanted damping level at the first and second vibrational mode. Larger damping also gives a smoother response surface, which makes the FORM iterations converge faster. An example fatigue damage contour is shown in Fig. 11 where two of the largest wave components are varied from 0 to 2π. The contour confirms that the fatigue damage is very sensitive to the wave phase angles.

For validation of the results, 10,000 simulations have been run for the different sea-states, using approximately 120 CPU hours for each condition with the detailed model. The validation plots are presented in Fig. 12. By varying the SCF in the fatigue calculations, it is found that the curvature in highly dependent on the fatigue limit of the bi-linear S-N curve. For sea-state 3, the stress amplitudes are mainly located above the fatigue limit. This results in the same exponent for almost all rainflow counted stress ranges for this sea-state and a close to Gaussian distributed fatigue damage, especially for wave loads only. For the smaller sea-states, only some stress ranges are exceeding the fatigue limit, resulting in a larger variation between the different seeds and more samples in the distribution tail. These processes are closer to Rayleigh or Weibull distributions.

The three presented methods for alternative fatigue damage estimation in Table 2 are fitted to the results from the wave only analysis by sea-state 1 and presented in Fig. 13. Here, 10 seeds are randomly drawn from the 10,000 existing simulations, and the different methods are applied. To conclude, the SL method and quadratic fit seems to represent the underlying distribution well, whereas the linear fit misses the distribution slightly, but may still be appropriate for finding the expected value since it crosses $\beta = 0$ almost exactly at $D/D_e = 1$.

Wave Loads Only

As an initial study, only wave forces was included in the model. To reduce the number of random variables, deterministic wave amplitudes are used and the simulation time is limited to 100 seconds, which gives a maximum of 35 insertions in **u**. However, by using (33), the number of variables are reduced to between 15 and 25, depending on the spectrum and significance threshold. The FORM evaluated design-points chosen for proper representation of the extremes are shown in Table 7.

The complete results for wave loads are shown in Fig. 14 with number of utilized seeds in the fatigue estima-

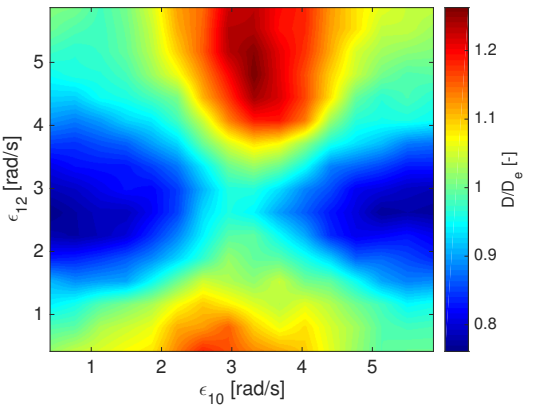

Figure 11. Example response surface by varying two wave component phase angles for sea-state 3

Table 7. FORM design-points for wave loads

Sea-state	$D_{\text{year,ext}}$	β_{FORM}
1	0.03	3.15
2	0.80	2.55
3	2.40	2.40

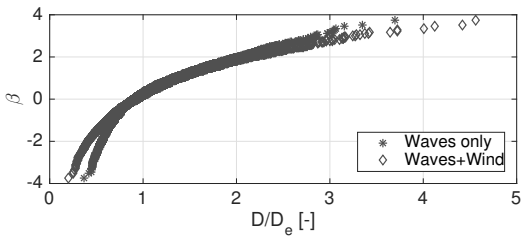

(a) Sea-state 1

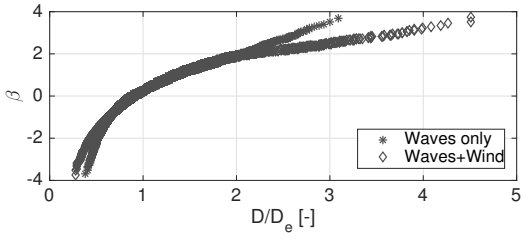

(b) Sea-state 2

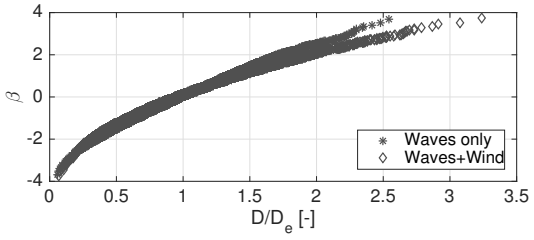

(c) Sea-state 3

Figure 12. Fatigue damage results with 10,000 simulations for each sea-state and loading condition

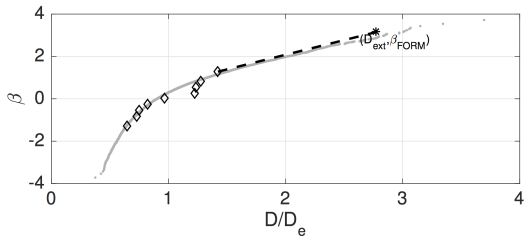

(a) Sum+linear fit

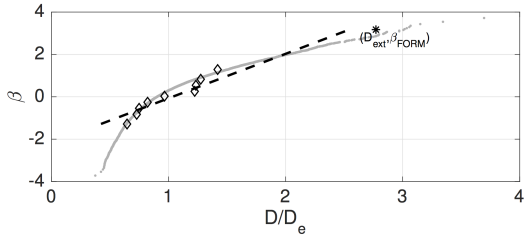

(b) Linear fit

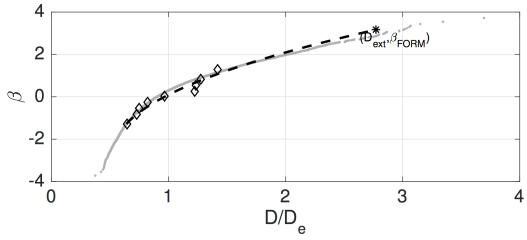

(c) Quadratic fit

Figure 13. Example fits using the three presented methods using wave loads only and 10 simulations with sea-state 1. Underlying distribution and the FORM evaluated point is plotted.

tion on the x-axis. For each number of seeds, $K = 300$ independent simulations are used to evaluate the mean fatigue and standard deviation. In most cases, the expected fatigue has converged after about 20 seeds for all methods. The most promising results are in sea-state 1 and 2, where the expected fatigue is converging quickly and the variance is lower than the variance using the conventional averaging, σ_C^2, defined as

$$\sigma_{C|N}^2 = \frac{1}{K}\sum_{i=1}^{K}(D_i - D_{C|N})^2 \tag{50}$$

where $D_{C|N}$ is the mean fatigue for N simulations. Note that the linear and quadratic fit provides the best results when accurately estimating the expected fatigue while having relatively low variance, which is the suggested benefit by using these methods. The SL method is most beneficial for small N, when the two last terms in (20) are still contributing significantly. Interestingly, the SL method does not provide a sufficiently large reduction in the variance, which is due to variations in the MCS point for linearizing the tail. For sea-state 3, no large improvements are seen in the uncertainty of the results. An explanation for this is that the conventional method is already estimating the fatigue quite accurately for a relatively small number of seeds.

For the FORM method to be preferable, the time used for finding β_{FORM} must be smaller than additional Monte Carlo simulations to obtain a smaller variance with the conventional method. For sea-state 3, this is clearly not feasible, but it may be beneficial for sea-state 1, considering that finding β_{FORM} consumes the same time as 40-60 simulations, depending on the initiation point. With a large difference between the detailed and simple model, the argument of curve-fitting is even stronger.

Wave- and Wind Loads

When including wind loads, the simulation model has proved to be slightly more non-linear resulting in larger fatigue damage variations as seen in Fig. 12. Therefore, it is expected that the presented methods will be even more efficient. However, the inclusion of wind loads leads to a dramatic increase in random variables. For a simulation time of 100s, as much as 135 random variables has to be used to avoid repetition of the environmental loads. Even though the number is reduced to about 90-110 by using (33), the computational efforts to find β_{FORM} are still significant, meaning more than 100 simulations with the detailed model. For demonstration of the method, results in Fig. 15 are found using the second largest points in Fig. 12 as the FORM design-points.

The complete results are shown in Fig. 15 using the same approach as for the case with only wave loads. Here, the results are very similar to what is observed in the wave load case. Reduction of the uncertainty is seen

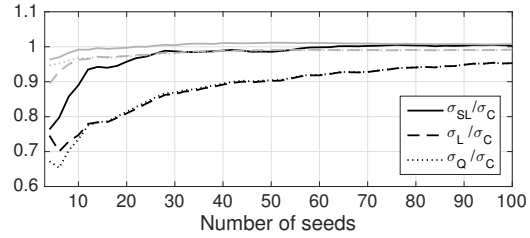

(a) Sea-state 1

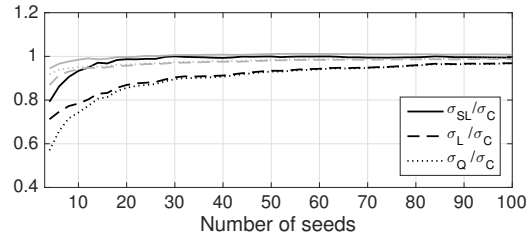

(b) Sea-state 2

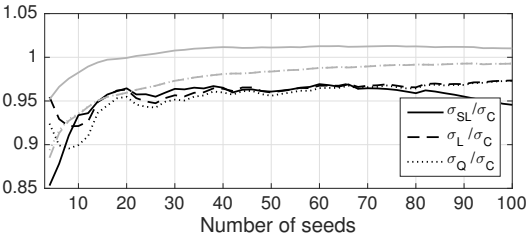

(c) Sea-state 3

Figure 14. Standard deviations of fatigue damage estimation given number of seeds (N) of 100s simulations with only wave loads. Gray lines are the mean fatigue normalized with true damage.

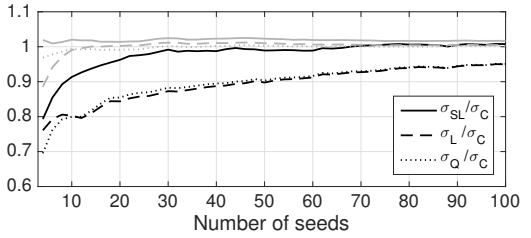

(a) Sea-state 1

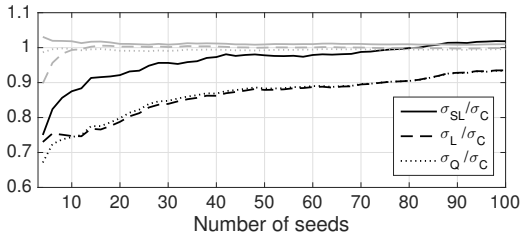

(b) Sea-state 2

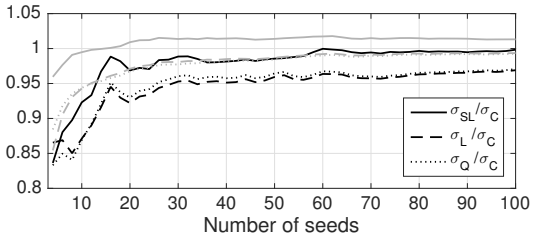

(c) Sea-state 3

Figure 15. Standard deviations of fatigue damage estimation given number of seeds (N) of 100s simulations with wind and wave loads. Gray lines are the mean fatigue normalized with true damage.

for small number of seeds with the curve-fitting methods, but not large enough to justify using significant computational efforts on the FORM analysis.

Conclusions

To conclude, the fatigue damage estimation using a FORM procedure may lead to a reduced uncertainty if the FORM design-point is properly found and contributes significantly to the integration. Especially the linear and quadratic curve fitting methods have proven more reliable that conventional averaging. It has been found that the standard deviation is reduced up to 30% for load cases where the fatigue damage distribution deviates from the normal distribution.

The multi-step FORM procedure might be computationally efficient in a wide range of applications if the simulation model can be simplified sufficiently. For the presented procedure applied to wind turbines to be computationally competing with the conventional average of simulations, β_{FORM} for D_{ext} has to be found with relatively small efforts, or be known from previous analyses by e.g. scaling with respect to the significant wave height (Jensen, 2011). A simpler linear model corresponding to a wind turbine model with a more sophisticated aerodynamic model should be used in future work to reduce computational efforts and evaluate the applicability and effectiveness of the presented methods.

Acknowledgement

This work has been carried out at the Centre for Autonomous Marine Operations and Systems at the Norwegian University of Science and Technology (NTNU AMOS). The Norwegian Research Council is acknowledged as the main sponsor of NTNU AMOS. This work was supported by the Research Council of Norway through the Centres of Excellence funding scheme, Project number 223254 - NTNU AMOS.

References

Bak, C., Zahle, F., Bitsche, R., Yde, A., Henriksen, L. C., Nata, A., and Hansen, M. H. (2013). Description of the DTU 10 MW Reference Wind Turbine. (July).

Burton, T., Sharpe, D., Jenkins, N., and Bossanyi, E. (2002). *Wind Energy Handbook*. John Wiley & Sons, Ltd.

DNV GL (2005). RP-C203 Fatigue design of offshore steel structures. Technical Report April.

DNV GL (2014). OS-J101 Design of Offshore Wind Turbine Structures. Technical report.

Faltinsen, O. M., Newman, J. N., and Vinje, T. (1995). Nonlinear wave loads on a slender vertical cylinder. *Journal of Fluid Mechanics*, 289:179.

Horn, J. T. H., Krokstad, J. R., and Amdahl, J. (2016). Hydro-Elastic Contributions to Fatigue Damage on a Large Monopile. *Energy Procedia*.

Jensen, J. J. (2011). Extreme value predictions using Monte Carlo simulations with artificially increased load spectrum. *Probabilistic Engineering Mechanics*, 26(2):399–404.

Jensen, J. J. (2015). Fatigue damage estimation in nonlinear systems using a combination of Monte Carlo simulation and the First Order Reliability Method. *Marine Structures*, 44:203–210.

Liu, P.-L. and Der Kiureghian, A. (1991). Optimization algorithms for structural reliability. *Structural Safety*, 9(3):161–177.

Madsen, H., Krenk, S., and Lind, N. (1986). *Methods of Structural Safety*. Prentice-Hall, Inc.

Moan, T. and Naess, A. (2013). *Stochastic Dynamics of Marine Structures*. Cambridge University Press.

Smilden, E. and Eliassen, L. (2016). Wind Model for Simulation of Thrust Variations on a Wind Turbine. *Energy Procedia*.

Tucker, M., Challenor, P., and Carter, D. (1984). Numerical simulation of a random sea: a common error and its effect upon wave group statistics. *Applied Ocean Research*, 6(2):118–122.

WAFO-group (2000). WAFO - A Matlab Toolbox for Analysis of Random Waves and Loads.

Zheng, X. Y., Moan, T., and Quek, S. T. (2006). Numerical simulation of non-Gaussian wave elevation and kinematics based on two-dimensional fourier transform. pages 1–6.

Zwick, D. and Muskulus, M. (2015). The simulation error caused by input loading variability in offshore wind turbine structural analysis. *Wind Energy*, 18(8).